Computer model for transient grating experiments and its application to analysis of $LiTaO_3$

Heather M. Perry and Thomas P. Dougherty
Department of Chemistry and Physics, Beaver College, Glenside, Pennsylvania 19038
(Received 9 July 1996)

A computer program is used to model transient grating experiments where two laser pulses induce a transient response in the sample and the time evolution of that response is monitored by the diffraction of a third pulse. The program is designed so that experimental conditions such as spot sizes, excitation angle, probe angle, relative pump and probe positions, and laser wavelength can be readily varied. The model accommodates acoustic and polariton excitations which travel significant distances during an experiment. This program is used to simulate and analyze transient grating experiments of A_1-symmetry polaritons in the ferroelectric crystal $LiTaO_3$. Previous experiments have used two different detection schemes for the scattered pulse, and two different models for the optic modes of $LiTaO_3$ were proposed. The simulations show that the discrepancies result from an experimental artifact in the heterodyne detection experiments, and both sets of experiments are consistent with one model for the crystal's optic modes. [S0163-1829(97)02109-7]

I. INTRODUCTION

With the development of pulsed lasers a wide range of transient grating experiments have become possible. A recent review of time-domain spectroscopy discusses many applications of transient grating spectroscopy.[1] In crystalline solids, this technique has been used to study transverse- and longitudinal-acoustic and optic modes. In liquids, molecular vibrations, reorientations, and longitudinal-acoustic modes have been observed, and transverse-acoustic modes have been found in glass-forming liquids near the glass transition.

The appropriate experimental conditions (angles between the excitation beams, excitation and probe spot sizes, etc.) depend on the type of excitation produced. This is particularly true for wave-vector-dependent (dispersive) excitations; in addition to a dependence of the observed frequency and decay rate on the grating wavelength, propagation of the transient excitation can significantly affect the results.[2]

A general computer model for transient grating experiments is presented here. It can be used to examine any type of material excitation, whether it is propagating or nonpropagating. With this model a range of experimental conditions can be rapidly evaluated and an appropriate set of conditions can be chosen. More importantly, the model can be used for the analysis of experimental results; it is a powerful tool for separating experimental artifacts from the physical quantities of interest.

To demonstrate the validity and utility of this model, transient grating experiments on A_1-symmetry phonon-polaritons in $LiTaO_3$ will be simulated. Phonon-polaritons are propagating excitations which allow for a thorough test of the model, and the results of transient grating experiments at a wide range of conditions have been published.[3–6] The interpretations of these experiments have produced two fundamentally incompatible models for the low-frequency A_1-symmetry optic modes of $LiTaO_3$. Impulsive stimulated scattering (ISS) experiments[3,4] found that the polariton was well described by a single damped harmonic oscillator response function at all wave vectors. However, the anomalous dispersion of the polariton decay rate was interpreted as evidence for a low-frequency relaxational mode. Transient grating experiments using a heterodyne detection technique[5,6] found instead that two damped harmonic oscillator response functions were required at wave vectors near 1000 cm^{-1}. This was interpreted as evidence of a previously unobserved 0.95 THz mode. The simulations below provide an explanation for the observed data and demonstrate that all the results are consistent with the first model for the optic modes of $LiTaO_3$.[4]

II. TRANSIENT GRATING MODEL

All Gaussian wave packets, laser pulses and material excitations are represented as properly weighted sums of plane waves. Notice that representing the excitation in this way places no restrictions on the type of excitation that can be analyzed. For propagating excitations (and the laser pulses), the frequency and decay rate of each plane wave is a function of wave vector. For nonpropagating excitations, the plane-wave frequency and decay rate are independent of wave vector. Except for differences in the dispersion of frequency and decay rate, all excitations are treated in the same manner.

In order to simplify the model and reduce the computation times required, the transient grating experiment is approximated in two dimensions. The excitation and probe beam wave vectors are restricted to the xy plane of a laboratory coordinate system and enter and exit the sample through faces of the sample which are parallel to the xz plane. The wave vectors of the transient grating produced are restricted to the xy plane as well. This approximation makes all of the laser pulses and the transient grating infinitely large in the z direction. To reproduce the correct spatial profile in the z direction for the laser pulses and the transient grating, each of these wave packets would need a distribution of wave-vector z components as well. This approximation greatly accelerates the calculations and should not significantly affect the results.

The scattering of one of the probe pulse's plane-wave components by one of the transient grating's plane-wave

components can be calculated by requiring that energy and momentum be conserved in the scattering event. For experiments in which the indices of refraction for both the probe and scattered pulses are the same (parallel polarizations or isotropic sample) and both pulses exit the same face of the sample, the conservation of energy requirement can be written in terms of the photon wave vectors in air (under these conditions, the phonon wave vector is determined by the photon wave vectors and scattering angle measured in air),[4]

$$k_s = k_i \pm \frac{\omega}{c}, \tag{1a}$$

where k_s is the wave-vector magnitude of scattered probe plane wave, k_i is the wave-vector magnitude of incident probe plane wave, ω is the frequency of grating excitation plane wave, and ''$\pm$'' is for the destruction or creation of a phonon. The general expression in terms of photon wave vectors in the sample is

$$\frac{k_s}{n_s} = \frac{k_i}{n_i} \pm \frac{\omega}{c}, \tag{1b}$$

where n_i and n_s are the indices of refraction for the incident and scattered pulses. Conservation of momentum requires that

$$k_{sx} = k_{ix} \pm q_x \tag{2a}$$

and

$$k_{sy} = k_{iy} \pm q_y, \tag{2b}$$

where k_{sx} is the x component of the scattered probe wave vector, k_{sy} is the y component of the scattered probe wave vector, k_{ix} is the x component of the incident probe wave vector, k_{iy} is the y component of the incident probe wave vector, q_x is the x component of the grating wave vector, q_y is the y component of the grating wave vector, and ''$\pm$'' is for the destruction or creation of a phonon. Photon wave vectors measured in air may be used instead of the values measured in the crystal when Eq. (1a) is applicable. Once q_x, q_y, ω, and k_i are chosen, there are only two pairs of solutions for k_{ix} and k_{iy} that satisfy the conservation of energy and momentum requirements; one corresponds to the destruction of a phonon and the other to the creation of a phonon.

In many transient grating experiments, the depth of the grating (throughout this paper, the y dimension) is limited by the thickness of the sample, rather than the region of overlap of the excitation pulses. The $LiTaO_3$ experiments modeled below[3–6] are examples where thin samples limit the depths of the transient gratings. For these experiments a further approximation is made. The width of the grating (the x dimension) is governed by the distribution of the x components of the excitation wave vectors, but no attempt is made to reproduce the depth of the grating (the y dimension) with a distribution of y components of the excitation wave vectors (the value of q_y used for each plane wave depends on ω because of conservation of energy and momentum considerations in the excitation process). Instead, the depth of the grating (assumed to be the same as the thickness of the sample) is modeled by relaxing conservation of momentum in the y direction in the following way. The expressions for conservation of energy and conservation of momentum in the x direction remain as shown in Eqs. (1) and (2a). The y component of the wave vector of the scattered wave, k'_{sy}, is calculated from the following equation:

$$(k'_{sy})^2 = k_s^2 - k_{sx}^2 \tag{3}$$

and the amplitude of the scattered field is proportional to

$$\mathrm{sinc}\left[\frac{(k'_{sy} - k_{sy})L}{2}\right], \tag{4}$$

where L is the thickness of the sample and

$$\mathrm{sinc}(x) = \frac{\sin(x)}{x}. \tag{5}$$

The sinc function is chosen to reproduce the square shape in the y direction imposed by the thin sample.[7] A Gaussian function for the scattered amplitude,

$$\text{amplitude} \propto e^{-(k'_{sy} - k_{sy})^2/\sigma^2} \tag{6}$$

was also examined; it produces a Gaussian rather than square shape to the y cross section of the grating, but it gives very similar results as the sinc function when the values of L and σ are chosen to produce gratings of similar thicknesses. Note that either a distribution of y-momentum components or the relaxed y-momentum conservation must be used to give a finite thickness to the grating. The relaxed y-momentum conservation method will be used in all examples in this paper.

The scattered pulse is calculated by scattering each of the probe pulse's plane-wave components off each of the transient grating's plane-wave components and summing the scattered waves. The scattered field, $C_s(x,y,t)$, has the following form:

$$C_s(x,y,t) = \sum_i E_i \cos(k_{sx,i}x + k_{sy,i}y - \omega_i t), \tag{7}$$

where the sum is over all scattered waves. By also calculating the following expression,

$$D_s(x,y,t) = \sum_i E_i \sin(k_{sx,i}x + k_{sy,i}y - \omega_i t) \tag{8}$$

the amplitude, $E_s(x,y,t)$, and phase, $\phi_s(x,y,t)$, of the scattered wave can be determined from

$$E_s = \sqrt{C_s^2 + D_s^2} \tag{9}$$

and

$$\phi_s = \tan^{-1}\left(\frac{D_s}{C_s}\right). \tag{10}$$

$E_s(x,y,t)$ and $\phi_s(x,y,t)$ will be useful for calculating experimentally observable quantities below.

In the simulations presented here, an impulsive excitation is used to initiate the material response. This is an appropriate approximation for most transient grating experiments, including the $LiTaO_3$ experiments simulated here. In some cases, however, it is the time dependence of the excitation that is of interest. For example, in transient thermal grating

experiments, it is the time-dependent conversion of the electronic excitation to a thermal excitation which is of interest.[8,9] The transient grating model can be modified to simulate an excitation with any time dependence by approximating the excitation with a series of properly weighted impulse forces.

Finally, the effects of finite probe pulse time resolution are neglected in the simulations presented below. For the ISS simulations, pulse convolution effects can be readily added, but adding pulse convolution to the heterodyne technique would slow the calculations significantly. At the wave vectors of interest for the simulations below (approximately 1000 cm^{-1}), the period of the polariton oscillation is approximately 1.0 ps, far longer than the probe pulse durations used in these experiments,[3–6] and pulse convolution effects are not significant.

III. APPLICATION OF THE MODEL TO A_1-SYMMETRY POLARITONS IN $LiTaO_3$

A. Inclusion of experimental conditions into the model

The transient grating used in a simulation is defined using several input parameters and a dispersion model for the grating excitation. In all of the examples presented below, the wave-vector-dependent sample response is determined from the model for A_1-symmetry polaritons in $LiTaO_3$ presented in Sec. V B of Ref. 4. This model includes one polar optic mode and a coupled relaxational mode. As shown in Fig. 5 of Ref. 4, this model and the more sophisticated model developed in the same section are indistinguishable in the low wave-vector region ($\approx$1000 cm^{-1}) where the heterodyne detection and ISS transient grating experiments differ most dramatically.[4,5] The $LiTaO_3$ model parameters used are: $\omega_1=0.0379$ fs^{-1}, $\Gamma_1=0.0027$ fs^{-1}, $\omega_L=0.0758$ fs^{-1}, $\varepsilon'_\infty=8.5$, $\tau=0.3$ ps, and $B^{1r}B^{r1}=3.2\times10^{-4}$ fs^{-2}. As noted above, different models can be readily substituted for this one to examine different materials.

The central grating wave vector is calculated from the central wavelength of the excitation pulses λ_e, and the angle between the excitation pulses (measured in air, not in the sample) θ_e. In the examples below, the central excitation wave vector is calculated assuming that the index of refraction in the sample is the same for both excitation pulses. This is appropriate for isotropic samples or parallel polarizations for the excitation pulses. When perpendicularly polarized excitation pulses are used in a birefringent sample, λ_e, θ_e, and the indices of refraction would be required to calculate the central wave vector.[10] The input value for the width (x dimension) of the grating is used to select the range of grating excitation wave vectors and their relative amplitudes. Experimentally, this value is determined from the x dimensions of the excitation laser pulses. The x position of the center of the grating (at $y=0$), the number of plane waves used to describe the grating excitation, and the thickness of the sample complete the description of the transient grating.

The probe pulse wavelengths are determined from the central wavelength λ_p, pulse duration τ_p, and the number of wavelengths m used to model the pulse. For each wavelength, a distribution of n different wave-vector directions is used. The distribution is determined by the input value for the probe spot size. Therefore, the probe pulse is the sum of $n\times m$ plane waves. The final probe parameters are the angle of incidence θ_p and the x position of the center of the probe at $y=0$.

The final considerations for modeling transient grating experiments involve the nature of the detection system. For ISS experiments, in which only light scattered by the grating reaches the detector, the signal is proportional to the square of the electric field at the detector. Since the detector is slow, it integrates the time response of the scattered pulse, and the signal is proportional to the peak value of E_s squared [see Eq. (9)]. The detector also integrates in the spatial dimensions. This is particularly important in cases such as Fig. 3 below, when the spatial profile of the scattered pulse is not Gaussian. To handle this situation, the scattered signal is integrated numerically along the x direction. The number of points used in the numerical integration is an input parameter.

For the heterodyne detection method,[5,6] both the inelastically scattered light from the transient grating and elastically scattered light from surfaces or defects interfere at the detector. The integrated intensity at the detector, I, is a function of the pulse scattered by the transient grating and the stray probe light:

$$I=\int_{-\infty}^{\infty}[E_p e^{-(t-t_0/\tau_p)^2}\cos(\omega_p t+\phi_p) + E_s e^{-(t-t_0/\tau_s)^2}\cos(\omega_s t+\phi_s)]^2 dt, \tag{11}$$

where ω_p is the central probe frequency, τ_p is the probe pulse duration, ϕ_p is the probe pulse phase, ω_s is the central scattered frequency, τ_s is the scattered pulse duration, ϕ_s is the scattered pulse phase, and t_0 is the time required for the peak of probe and scattered pulse to travel from the sample to the detector. This expression for I can be rearranged to have the form $I=I_1+I_2$, where

$$I_1=E_p^2\int_{-\infty}^{\infty}e^{-2(t-t_0/\tau_p)^2}\cos^2(\omega_p t+\phi_p)dt + E_s^2\int_{-\infty}^{\infty}e^{-2(t-t_0/\tau_s)^2}\cos^2(\omega_s t+\phi_s)dt \tag{12a}$$

and

$$I_2=2E_pE_s\int_{-\infty}^{\infty}e^{-(t-t_0/\tau_p)^2}e^{-(t-t_0/\tau_s)^2} \times\cos(\omega_p t+\phi_p)\cos(\omega_s t+\phi_s)dt. \tag{12b}$$

The expression for I_1 is readily evaluated,

$$I_1=E_p^2\frac{\tau_p}{2}\sqrt{\frac{\pi}{2}}+E_s^2\frac{\tau_s}{2}\sqrt{\frac{\pi}{2}} \tag{13}$$

and is the sum of the intensities of the two pulses when considered independently. The heterodyne term or interference effects between the two pulses are contained in the expression for I_2. Evaluating the expression for I_2 gives

$$I_2 = E_p E_s \cos(\phi_p - \phi_s)\cos(\Delta\omega t_0)\frac{\sqrt{\pi}}{a} e^{-(\Delta\omega)^2/4a^2}, \tag{14a}$$

where

$$\Delta\omega = \omega_p - \omega_s \tag{14b}$$

and

$$a = \frac{\sqrt{\tau_p^2 + \tau_s^2}}{\tau_p \tau_s}. \tag{14c}$$

When calculating the signal for a simulation, several of these terms can be neglected as constants. The elastically scattered field E_p needs to be constant or the heterodyne experiment is impossible. $\sqrt{\pi}$ and a are clearly constants, and the exponential term is nearly constant during an experiment. It is approximately equal to one when the excitation and probe pulses are short compared to the grating oscillation period (at small wave vectors) and decreases as the frequency of the grating excitation increases (at larger wave vectors). This exponential term reflects one way in which the experimental time resolution affects the observed signal. The remaining terms must be calculated from the model. E_s [Eq. (9)], the amplitude of the scattered field, depends primarily on the phase matching angle of the probe pulse, the spatial overlap of the probe and grating and the grating amplitude. The first cosine term, $\cos(\phi_p - \phi_s)$, oscillates at the frequency of the transient grating response (but only for propagating excitations like polaritons). The values of ϕ_p and ϕ_s [Eq. (10)] are calculated at the same point in the sample. The second cosine term, $\cos(\Delta\omega t_0)$, depends on the difference in frequency between the two pulses and the time required for the pulses to travel from the sample to the detector. It will be shown below that neither $\Delta\omega$ nor t_0 are constant during an experiment. Under the conditions of the simulations presented here, the changes in $\Delta\omega$ are more important than the changes in t_0.

In order to calculate ω_s (and $\Delta\omega$) as accurately as possible, the phase of the scattered pulse, ϕ_s, is calculated approximately 180 times over a 375 fs period (approximately twice per cycle of the electric field). Since this approach is time consuming, an additional simplification is made when calculating the signal for this experiment. The initial transient grating formed in these experiments is actually the sum of two counter-propagating wave packets, and the probe pulse interrogates a region next to and only partially overlapping the initial grating position.[5,6] As the experiment progresses, one of the wave packets propagates into (and eventually out of) the probed region and the other leaves the probed region and has no effect on the scattered signal after the first 2 ps.[5] The approximation made is to consider only the wave packet which propagates into the probe region and neglects the wave packet which propagates away from the probe region. Oscillations at twice the polariton frequency [observed experimentally (Fig. 1, Ref. 5)], will not be reproduced in the simulations, but the more important beating pattern (at about 5 ps) is reproduced. Including both wave packets can produce distinctly non-Gaussian spatial profiles on the scattered pulse in the first 1 to 2 ps of the simulations. Since the determination of ω_s makes the calculation of the signal in this case quite lengthy, including a spatial integration at the detector (analogous to what was done for the ISS experiment above) to examine an aspect of the experiment which is not central to resolving the differences with the ISS experiments was rejected as too time consuming.

In all of the simulations of heterodyne detection shown below, the value for t_0 in the equation for I_2 is determined by placing the detector 1.0 cm from the sample. While this distance is certainly much shorter than what is practical in the laboratory, the equation for I_2 assumes that the time for the scattered and stray light to reach the sample are exactly the same. In practice, the exact nature of the light collection optics (a combination of lenses and mirrors) will have an effect on the heterodyne signal by causing the two pulses (with different central frequencies) to take different lengths of time to reach the detector. Since the details of the collection optics used for the heterodyne experiments are not available, the simplest case with no optics is used.

B. Simulations of ISS experiments

In most of the ISS experiments,[3,4] cylindrical focusing of the excitation pulses was used to produce transient gratings which are large (1.2 mm) in the x dimension. The probe pulse has an approximately 10 times smaller width and is focused on the center of the grating. By this choice of experimental conditions, the counter-propagating wave packets are much longer in the direction of travel than the distance traveled before the excitation decays. Similar experimental conditions have been demonstrated to be effective in eliminating excitation propagation effects for acoustic gratings.[11] In all of the ISS experiments, no evidence was found for anything other than a single (wave-vector dependent) damped harmonic oscillator response at all wave vectors.

A series of simulations were produced with the following set of experimental conditions: grating width [full width at half maximum (FWHM)]=3.3 mm, probe pulse width (FWHM)=133 μm, probe pulse duration=100 fs, the x position of the centers of the probe pulse and the initial transient grating at the sample are the same, 29 plane waves define the grating, (21×11) plane waves define the probe, 2.0 mm sample thickness, and the spatial numerical integration of the scattered signal is approximated with 11 points. With the excitation and probe pulses at 615 nm, angles of incidence for the beams at the sample from 0.00134 to 0.049 radians were used to simulate 13 different experiments with central polariton wave vectors q, from 281 to 10 290 cm^{-1}. Three examples with wave vectors near 1000 cm^{-1} (to be compared with the heterodyne simulations below) are shown in Fig. 1. All of the ISS simulations are well fit by a single damped harmonic oscillator; the simulation and fit would be indistinguishable if both were included in the same figure.

As a test of the transient grating model and the suitability of ISS experiments for measuring polariton properties, the wave-vector-dependent frequencies ω and decay rates γ from the fits to the simulated experiments are compared in Fig. 2 to the polariton dispersion relation used in the model. The excellent agreement is a self-consistency check and indicates that the results of ISS experiments at these conditions can be directly related to the polariton response.

As a further test of the transient grating model, an ISS experiment with much smaller spot sizes for the excitation pulses was simulated. The results of such an experiment

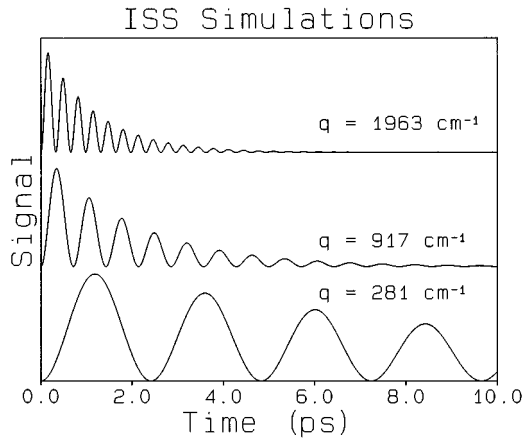

FIG. 1. Simulations of A_1-symmetry ISS experiments in $LiTaO_3$ at three different wave vectors. The material and excitation parameters are described in the text. At each wave vector, the simulation is well described by a single damped harmonic oscillator response function. For comparison to experimental results, see Fig. 9 of Ref. 3 and Fig. 2 of Ref. 4.

have been published,[3] and the signal is dramatically different from what is obtained with wide excitation pulses. The observed nonexponential decay of the signal was attributed to wave packet propagation effects. A simulated experiment with conditions similar to those used for the data in Fig. 8 of Ref. 3, is shown in Fig. 3. The simulated data successfully reproduce the experimentally observed nonexponential decay.

These simulations indicate that the proposed transient grating model can reproduce the results of ISS experiments in $LiTaO_3$ as a function of wave vector and excitation width. Since the dispersion relation used in initializing the transient grating wave packets is the only aspect of the model specific to $LiTaO_3$, any ISS experiment can be simulated with the model as long as an appropriate dispersion relation is substituted for the one used here.

C. Simulations of heterodyne detection experiments

The experimental conditions assumed for these simulations are similar to those reported in Ref. 6: grating width (FWHM)=250 μm, probe pulse width (FWHM)=250 μm, probe pulse duration=100 fs, the x position of the centers of the probe pulse and the initial transient grating are offset by 260 μm, 29 plane waves define the grating, (21×11) plane waves define the probe and 2.0 mm sample thickness. With the excitation and probe pulses at 615 nm, angles of incidence for the pump beams at the sample from 0.00123 to 0.049 radians were used to simulate 16 different experiments with central polariton wave vectors q from 257 to 10 290 cm^{-1}. The angle of incidence for the probe beam was chosen to be zero. This choice was suggested by Fig. 1 of Ref. 6. Another reference suggests a different probe orientation,[5] but it produces no qualitative difference in the simulations; at a fixed excitation wave vector, the primary difference observed from changing the angle of incidence of the probe is an overall decrease in signal amplitude as the probe angle moves away from the Bragg angle.

In Fig. 4, three simulations of heterodyne detection experiments in $LiTaO_3$ (using the same wave vectors as the

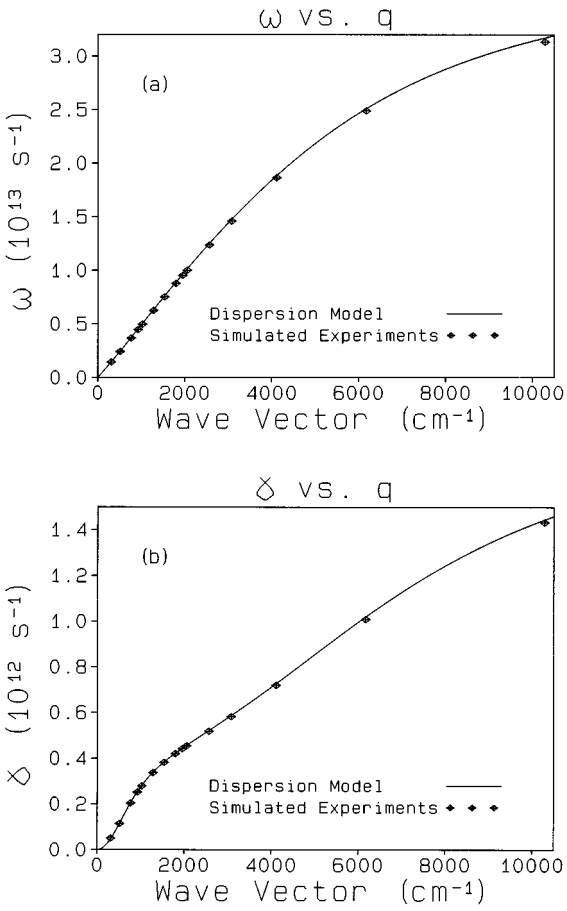

FIG. 2. The wave-vector dependence of the polariton frequency, ω, determined from the ISS simulations are compared to the dispersion model for $LiTaO_3$ used to produce the simulations in (a). The wave-vector dependence of the decay rate γ from the simulations and dispersion model are shown in (b). For comparison to experimental results, see Fig. 5 of Ref. 4.

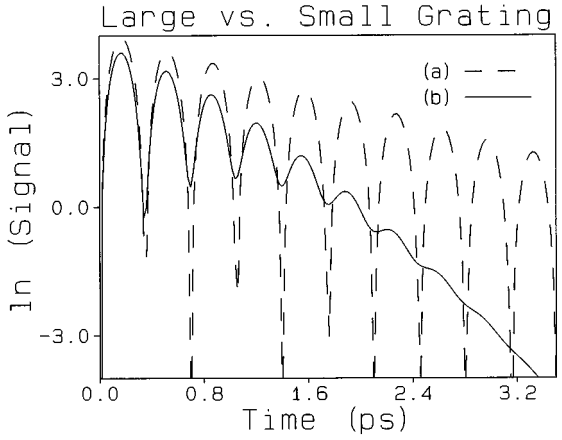

FIG. 3. Simulations at q=1839 cm^{-1} with (a) a 3.3 mm wide grating and (b) a 133 μm wide grating are shown. There is no significant difference in the observed frequencies for the two simulations, but there is a nonexponential decay of the signal for the small grating experiment which is not observed in the large grating experiment. Similar polariton wave-packet propagation effects in ISS experiments with small excitation spot sizes have been reported in Fig. 8 of Ref. 3.

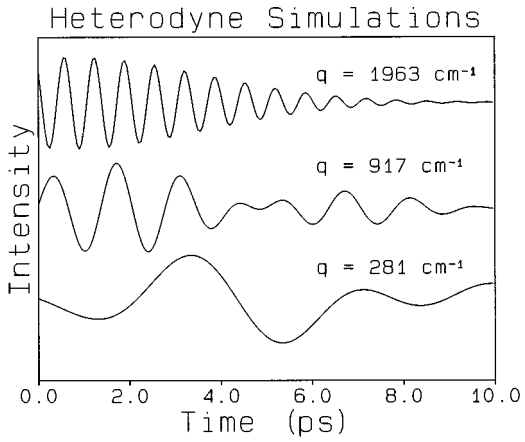

FIG. 4. Simulations of A_1-symmetry heterodyne detection experiments in $LiTaO_3$ at three different wave vectors. The material and excitation parameters are described in the text. At $q=917$ cm^{-1}, a beating pattern in the simulated data is seen. For comparison to experimental results, see Fig. 1 of Ref. 5.

three ISS simulations in Fig. 1) are shown. As expected, there are pulse propagation effects (similar to the ISS experiment in Fig. 3), and the signal oscillates at the polariton frequency, ω (rather than 2ω as in the ISS experiments). There is one significant difference between these simulations and the ISS simulations in Fig. 1; the signal response cannot be described as a single damped harmonic oscillator at all wave vectors. This can be seen by the beating pattern in the simulation at $q=917$ cm^{-1} and in the Fourier transform of this simulation shown in Fig. 5. The experimental results presented in Figs. 1 and 2 of Ref. 5 show a similar wave-vector dependence, with the most pronounced beating pattern at $q=1010$ cm^{-1}.

The beating pattern has been cited as evidence of an additional transverse-optic phonon at 0.95 THz.[5,6] This additional phonon cannot be the explanation for the beating pattern observed in the simulations (Fig. 4) because the dispersion model used for $LiTaO_3$ does not include this mode.[4] The form of the heterodyne simulations can be understood by reexamining Eq. (14a), the function used to calculate the signal. One of the cosine terms depends on $\Delta\omega$, which is the difference in frequency between the probe and scattered pulses, ω_p and ω_s, respectively; ω_p is independent of the time delay between the pump and probe pulses, but ω_s is not. Therefore, $\Delta\omega$ changes during an experiment. Since ω_s is one of the variables saved at each time step during a simulation, it is easy to calculate $\Delta(\Delta\omega)$, the difference between the largest and smallest values of ω_s calculated during the first 10 ps of an experiment, as a function of wave vector. The choice of 10 ps was made to coincide with the duration of spatial overlap of the probe with the propagating grating wave packet. As shown in Fig. 6, $\Delta(\Delta\omega)$ peaks at wave vectors where the beating pattern is most pronounced (just below 1000 cm^{-1}), and it is in this wave-vector region that changes in $\cos(\Delta\omega t_0)$ are most significant. At 917 cm^{-1}, $\Delta\omega t_0$ changes by approximately $3\pi/2$ in the first 10 ps with the detector 1.0 cm from the sample (t_0 is a function of this distance). Note that the magnitude of $\Delta(\Delta\omega)$ is sensitive to the grating spot size. At $k=917$ cm^{-1}, increasing the spot size from the value used in these simulations 250 μm to 375 μm decreases $\Delta(\Delta\omega)$ by a factor of 3. Doubling the size to 500 μm decreases $\Delta(\Delta\omega)$ by a factor of 30.

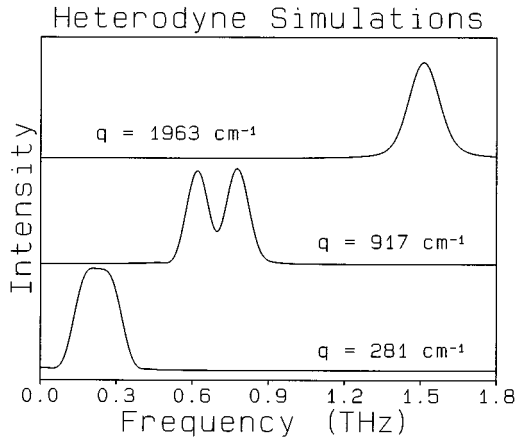

FIG. 5. Fourier transforms of the simulations in Fig. 4. The beating pattern seen in the time-domain simulation at $q=917$ cm^{-1} corresponds to a frequency-domain response with two peaks. For comparison to experimental results, see Fig. 2 of Ref. 5.

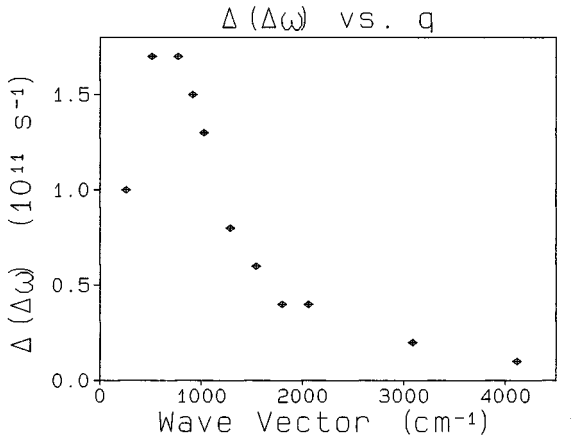

FIG. 6. The change in $\Delta\omega$ [Eq. (14b)] during the first 10 ps of a heterodyne detection experiment, $\Delta(\Delta\omega)$, is plotted as a function of excitation wave vector q. All experimental parameters except for q are identical to those used to produce the simulations in Fig. 4. Since ω_p is constant, all of the time dependence in $\Delta\omega$ is in ω_s, the frequency of the inelastically scattered probe pulse. The dependence of $\Delta\omega$ on the excitation/probe delay is the primary cause of the beating patterns seen in the heterodyne detection simulations.

In the simulations presented here, changes in $\Delta\omega$ are the most significant source of changes in $\cos(\Delta\omega t_0)$. This would not necessarily be true if more elaborate signal collection optics were used. As discussed above, introduction of lenses and mirrors after the sample invalidates the approximation that t_0, the time required for the pulses to travel from the sample to the detector, be the same for the scattered and stray light. The time required for the scattered light to reach the detector depends on the path the light takes from the sample to the detector. This path is not independent of the pump-probe delay time. $\Delta\theta$, the maximum change in the scattering angle during the first 10 ps of an experiment [analogous to $\Delta(\Delta\omega)$ above] also peaks at wave vectors below 1000 cm^{-1} (Fig. 7). While not significant in these simulations, variation

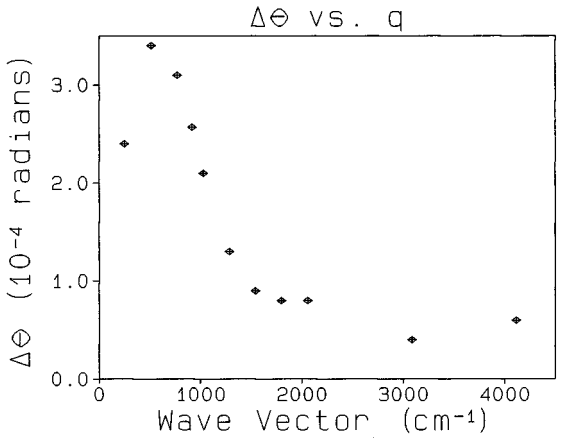

FIG. 7. The change in θ, the scattering angle of the probe pulse, during the first 10 ps of a heterodyne detection experiment, $\Delta\theta$, is plotted as a function of excitation wave vector q. All experimental parameters except for q are identical to those used to produce the simulations in Fig. 4. The effect of $\Delta\theta$ on the simulations shown here is quite small, but could be significant if the detector were moved farther from the sample and a series of lenses and mirrors was used to collect the light.

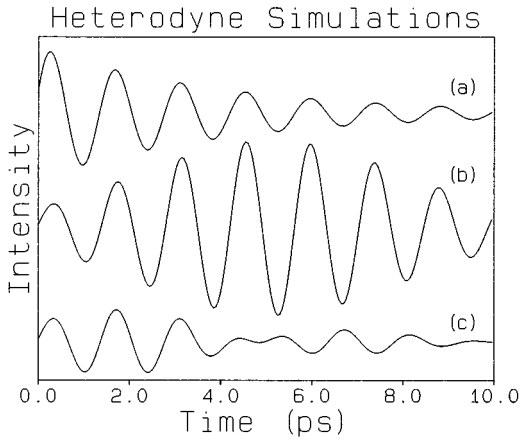

FIG. 8. Simulations of heterodyne detection experiments at $q=917\ \mathrm{cm}^{-1}$. For each simulation, all experimental parameters are identical to those used to produce the simulations in Fig. 4 except as noted below. (a) The size of the grating excitation is increased from 250 μm to 3.3 mm (FWHM). (b) The decay rate of the polariton at all wave vectors is set equal to zero. (c) Identical to the simulation at $q=917\ \mathrm{cm}^{-1}$ in Fig. 4.

in θ could be very important when considering more realistic light collection optics and their effects on the observed signal.

While the time dependences of $\Delta(\Delta\omega)$ and $\Delta\theta$ observed in the simulations can explain the observed beating patterns, it is important to understand the physical origins of this behavior. Since the polariton decay rate is a function of q (Refs. 3 and 4) and a wave packet with finite spatial dimensions must contain polaritons with a range of wave vectors, it is not always possible to define a wave-packet decay rate. Instead, the different wave-vector components decay at different rates, and the grating wavelength changes as the wave packet evolves in time. This change in the grating wavelength is observed in the time dependences of $\Delta(\Delta\omega)$ and $\Delta\theta$. Experimentally, the magnitudes of $\Delta(\Delta\omega)$ and $\Delta\theta$ depend on the central excitation wave vector, the width of the excitation and the dispersion relation for the material excitations. The dependence on the central excitation wave vector (the wavelength and scattering angle for the excitation pulses) is shown in Figs. 6 and 7. A simulation of the heterodyne experiment at $q=917\ \mathrm{cm}^{-1}$ with the same parameters as before except for increasing the width of the excitation from 250 μm to 3.3 mm (decreasing the range of wave vectors excited) is shown in Fig. 8(a). Comparing to the earlier simulation in Fig. 4 [and Fig. 8(c)] $\Delta(\Delta\omega)$ and $\Delta\theta$ are reduced by factors of 26 and 16, respectively. This has a dramatic effect on the simulation; the beating pattern is no longer observed. Unfortunately, it is not possible to perform a heterodyne experiment under these conditions. The two counterpropagating excitation wave packets will decay before they are spatially separated (the simulation ignores one of the wave packets). The dependence of the heterodyne signal on the dispersion relation can be seen in Fig. 8(b). In this simulation at $q=917\ \mathrm{cm}^{-1}$, the conditions are the same as for the simulations in Fig. 4 except that the decay rate of all excitations is set to zero. Once again, the beating pattern disappears. In this case, $\Delta(\Delta\omega)$ and $\Delta\theta$ are approximately 200 times smaller than the values shown in Figs. 6 and 7. Notice that the propagation of the grating wave packet into and out of the probed region is clearly observed in Fig. 8(b), but is not significant in the large grating simulation in Fig. 8(a). In the heterodyne experiments[5,6] at wave vectors near 1000 cm^{-1}, the excitation is sufficiently small (the range of excited wave vectors is sufficiently large) and the wave-vector dependence of the decay rate is sufficiently large that the time dependence of $\Delta(\Delta\omega)$ and $\Delta\theta$ must be considered in the analysis. In contrast, the ISS experiments which used large excitations (a narrow range of excitation wave vectors) do not exhibit these effects at any wave vector.

IV. CONCLUSION

The model presented above successfully reproduces the results of transient grating experiments in $LiTaO_3$ at a variety of experimental conditions. Since the only aspect of the model specific to $LiTaO_3$ is the polariton dispersion relation, the model is applicable to transient grating experiments in any sample for which the wave-vector dependence of the excitation is known or can be estimated.

In addition, the apparent incompatibility of the ISS and heterodyne $LiTaO_3$ experiments has been resolved. These simulations of the experiments in $LiTaO_3$ demonstrate that all transient grating experiments, heterodyne experiments and ISS experiments with large and small gratings, are consistent with the model for A_1-symmetry modes presented in Ref. 4. An alternative model which includes a resonance at 0.95 THz (Refs. 5 and 6) is based on inappropriate analysis of the heterodyne detection data. While further study is required, the analysis presented here also raises doubts about the interpretation of heterodyne experiments in other materials.[12]

It should be noted that the predictions made by the model can be readily tested. The signal observed in heterodyne experiments, described by Eq. (14a), depends on $\cos(\Delta\omega t_0)$. The time required for the scattered and heterodyne pulses to

reach the detector t_0 can be varied by moving the detector position. Doubling the distance from the sample to the detector should double the beating frequency. When performing this test, special care must be taken with the light collection optics. Equation (14a) assumes that the scattered and heterodyne pulses take exactly the same length of time to reach the detector. Since the two pulses have different central frequencies, any dispersive optic makes that approximation invalid. Very small differences in propagation times are significant because the period of the red light used in the $LiTaO_3$ experiments is about 2 fs. As a result, lenses after the sample can drastically complicate the calculation of the heterodyne signal.

The model presented here assumes that the grating thickness is determined by the thickness of the sample rather than the spatial overlap of the excitation pulses and that a two-dimensional representation of the experiment is sufficient. Modifications of the model to simulate experiments on ''thick'' samples and to produce a three-dimensional simulation are currently under investigation.

ACKNOWLEDGMENTS

We would like to thank Joseph C. Pearce for his assistance in writing the software and Beaver College for its support of this research.

[1] L. Dhar, J. A. Rogers, and K. A. Nelson, Chem. Rev. **94**, 157 (1994).
[2] Y.-X. Yan and K. A. Nelson, J. Chem. Phys. **87**, 6240 (1987).
[3] T. P. Dougherty, G. P. Wiederrecht, and K. A. Nelson, J. Opt. Soc. Am. B **9**, 2179 (1992).
[4] G. P. Wiederrecht, T. P. Dougherty, L. Dhar, and K. A. Nelson, Phys. Rev. B **51**, 916 (1995).
[5] H. J. Bakker, S. Hunsche, and H. Kurz, Phys. Rev. Lett. **69**, 2823 (1992).
[6] H. J. Bakker, S. Hunsche, and H. Kurz, Phys. Rev. B **48**, 13 524 (1993).
[7] E. Hecht and A. Zajac, *Optics* (Addison-Wesley, Reading, MA, 1979), pp. 211–213.
[8] E. J. Heilweil and R. M. Hochstrasser, J. Chem. Phys. **82**, 4762 (1985).
[9] L. Genberg, Q. Bao, S. Gracewski, and R. J. D. Miller, Chem. Phys. **131**, 81 (1989).
[10] T. P. Dougherty, G. P. Wiederrecht, K. A. Nelson, M. H. Garrett, H. P. Jenssen, and C. Warde, Phys. Rev. B **50**, 8996 (1994).
[11] L.-T. Cheng and K. A. Nelson, Phys. Rev. B **37**, 3603 (1988).
[12] H. J. Bakker, S. Hunsche, and H. Kurz, Phys. Rev. B **50**, 914 (1994).